

High-Efficiency Measurement of an Artificial Atom Embedded in a Parametric Amplifier

A. Eddins,^{1,2,*} J. M. Kreikebaum,^{1,2} D. M. Toyli,^{1,2} E. M. Levenson-Falk,^{1,2,†} A. Dove,^{1,2}
W. P. Livingston,^{1,2} B. A. Levitan,³ L. C. G. Govia,^{4,‡} A. A. Clerk,⁴ and I. Siddiqi^{1,2}

¹Quantum Nanoelectronics Laboratory, Department of Physics,
University of California, Berkeley, California 94720, USA

²Center for Quantum Coherent Science, University of California, Berkeley, California 94720, USA

³Department of Physics, McGill University, Montreal, Quebec H3A 2T8, Canada

⁴Institute for Molecular Engineering, University of Chicago, Chicago, Illinois 60637, USA

 (Received 13 June 2018; revised manuscript received 2 September 2018; published 7 January 2019)

A crucial limit to measurement efficiencies of superconducting circuits comes from losses involved when coupling to an external quantum amplifier. Here, we realize a device circumventing this problem by directly embedding an artificial atom, comprised of a transmon qubit, within a flux-pumped Josephson parametric amplifier. This configuration is able to enhance dispersive measurement without exposing the qubit to appreciable excess backaction. Near-optimal backaction is obtained by engineering the circuit to permit high-power operation that reduces information loss to unmonitored channels associated with the amplification and squeezing of quantum noise. By mitigating the effects of off-chip losses downstream, the on-chip gain of this device produces end-to-end measurement efficiencies of up to 80%. Our theoretical model accurately describes the observed interplay of gain and measurement backaction and delineates the parameter space for future improvement. The device is compatible with standard fabrication and measurement techniques and, thus, provides a route for definitive investigations of fundamental quantum effects and quantum control protocols.

DOI: [10.1103/PhysRevX.9.011004](https://doi.org/10.1103/PhysRevX.9.011004)

Subject Areas: Condensed Matter Physics,
Quantum Physics,
Quantum Information

I. INTRODUCTION

The sum of interactions between a quantum system and all environmental channels produces a continuous flow of quantum information into the environment, causing dephasing at a rate Γ_ϕ . For a two-level qubit described by $\hat{\sigma}_z$ and measured along that axis, one may define the fraction of this information flux experimentally captured per unit time to be the measurement efficiency $\eta_{\text{meas}} = \Gamma_{\text{meas}}/2\Gamma_\phi$, a critical parameter for continuous quantum measurements, where Γ_{meas} represents the rate at which the experimentalist learns about $\hat{\sigma}_z$ and is defined such that η_{meas} ranges from

0 to 1. The use of off-chip superconducting parametric amplifiers has enabled a variety of experiments investigating quantum measurement dynamics [1–6], with improvements in efficiency reported using multijunction circuits [7]; the remaining approximately 30% of the information is typically lost in dissipative elements such as circulators. Contemporary mitigation strategies include the development of superconducting circulators and directional amplifiers [8–14].

Here, we investigate a novel light-matter interaction using a minimal circuit architecture which provides on-chip parametric gain through the integration of a standard Josephson parametric amplifier (JPA) with the qubit in a configuration we dub the qubit parametric amplifier (QPA), removing virtually all preamplification loss. Previous demonstrations with on-chip amplifiers have leveraged the bifurcation dynamics of a nonlinear resonator [15–17]. In contrast, the QPA implements on chip the parametric mode of operation that has been widely applied in continuous measurements of qubits. This scheme presents a novel challenge, as the *in situ* microwave amplification and squeezing opens a parasitic measurement channel inducing excess dephasing. We model and characterize this backaction in detail and successfully mitigate it via a weakly nonlinear design permitting fast measurement, producing steady-state efficiencies as high as $\eta_{\text{meas}} = 0.80$ with

*To whom correspondence should be addressed.

aeddins@berkeley.edu

†Present address: Department of Physics and Astronomy, University of Southern California, Los Angeles, California 90089, USA.

‡Present address: Raytheon BBN Technologies, 10 Moulton Street, Cambridge, Massachusetts 02138, USA.

Published by the American Physical Society under the terms of the [Creative Commons Attribution 4.0 International license](https://creativecommons.org/licenses/by/4.0/). Further distribution of this work must maintain attribution to the author(s) and the published article's title, journal citation, and DOI.

direction for further improvement. The state-of-the-art measurement efficiencies provided by this device could be used to improve weak-measurement schemes such as continuous quantum error correction [18] and adaptive coherent control in applications such as quantum sensing [19]. Additionally, devices similar to the QPA could be used to explore novel quantum simulations and generate enhanced qubit-cavity couplings [20].

A schematic of our experiment appears in Fig. 1(a). The QPA consists of a transmon qubit [21] dispersively coupled to a JPA. A microwave readout tone at frequency ω_{QPA} reflects off the QPA, acquiring qubit-state information. A pump tone of the form $\cos[2(\omega_{\text{QPA}}t + \Phi)]$ applied to the pump port of the QPA concurrent with the readout modulates the QPA resonance frequency, producing on-chip phase-sensitive amplification of the measurement field. Adjusting Φ , the phase of the pump tone relative to the readout tone, changes which field quadrature is amplified and which is squeezed. The output of the QPA is then routed by microwave circulators to additional amplification stages including a second, off-chip JPA and a superconducting Josephson traveling-wave parametric amplifier (JTWPA) [22] en route to room-temperature demodulation and digitization. By acting as a phase-sensitive preamplifier before the JTWPA, which necessarily adds at least half a photon of noise in standard phase-preserving operation, the off-chip JPA reduces the amount of on-chip gain required for high efficiency.

A circuit diagram and false-color photographs of the QPA are shown in Figs. 1(b) and 1(c). The on-chip JPA design is similar to that of some off-chip JPAs [23,24], consisting of an interdigitated capacitor in parallel with a combination of

geometric and Josephson inductance to form an LC resonator (purple) whose frequency ω_{QPA} tunes with the flux applied through the pair of superconducting quantum interference device (SQUID) loops. A superconducting coil housed below the chip enables static tuning of ω_{QPA} , while a pump applied via the flux line (cyan) modulates ω_{QPA} to produce parametric gain. Some variation in the circuit parameters occurred as data were acquired over the course of multiple cooldowns; we give representative parameter values here and list precise values for each data set in Appendix A 2. The QPA resonator has a zero-flux frequency of $\omega_{\text{QPA,max}}/2\pi = 6.970$ GHz; we tune this down to $\omega_{\text{QPA}}/2\pi \leq 6.740$ GHz to increase the modulation amplitude produced by the flux pump. Coupling capacitors and a 180° microwave hybrid couple the resonator to the readout transmission line with an effective $\kappa_{\text{ext}}/2\pi = 25.7$ MHz $\gg \kappa_{\text{int}}/2\pi$. The transmon qubit (red) resonates at $\omega_q/2\pi = 4.271$ GHz and is capacitively coupled to the on-chip JPA with dispersive interaction strength $\chi/2\pi = 1.9$ MHz, with the convention that the ac Stark shift changes ω_q by $2\chi\bar{n}$. The paddle design of the qubit is chosen to reduce loss due to electromagnetic participation of the surface-vacuum interface, and a floating radiation shield (white) suppresses radiative decay of the qubit into other environmental modes. The measured lifetime $T_1 = 4.2(8)$ μs is near the expected Purcell-decay-limited value $T_1 \approx 6$ μs , which could be improved in future designs via integration of a Purcell filter [25].

In the dispersive approximation and in the frame rotating at ω_{QPA} , the internal QPA dynamics can be described by the Hamiltonian

$$\hat{H}_{\text{QPA}} \approx \frac{\hbar}{2} [\Delta + 2\chi(\hat{a}^\dagger \hat{a} + 1/2)] \hat{\sigma}_z + \frac{i\lambda}{2} (\hat{a}^{\dagger 2} - \hat{a}^2), \quad (1)$$

with $\Delta = \omega_q - \omega_{\text{QPA}}$. The first of the two terms is the familiar dispersive Hamiltonian that also describes the more common case of readout using a linear resonator. The second term describes the on-chip, phase-sensitive gain process, where λ is set by the flux-pump strength and would equal the rate of squeezing if there were no dissipation ($\kappa = 0$). A succinct theoretical analysis of the system is given in Appendix B, with further details available in Ref. [26].

II. MEASUREMENT BACKACTION WITH ON-CHIP GAIN

As in conventional qubit measurement setups, the dispersive interaction encodes information about the $\hat{\sigma}_z$ component of the qubit state into the mean value of one quadrature of the output field, which we refer to as the signal quadrature Q . This interaction necessarily dephases the qubit, as the intrinsic amplitude fluctuations of the measurement field produce a fluctuating ac Stark shift of the qubit frequency. We denote the total dephasing rate of the qubit as $\Gamma_\phi \geq \Gamma_{\phi,\text{QL}}$, where $\Gamma_{\phi,\text{QL}}$ represents quantum-limited backaction. High η_{meas} requires this

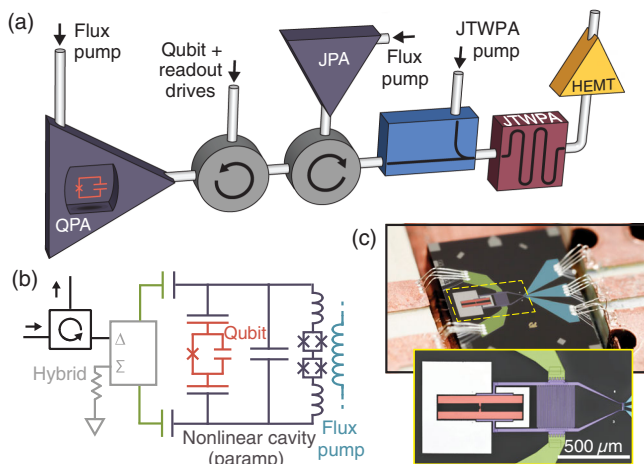


FIG. 1. (a) Simplified experimental setup. The QPA consists of a transmon qubit dispersively coupled to a JPA acting as the readout resonator. A coherent measurement tone reflects off the QPA, carrying qubit-state information to a second, off-chip JPA followed by a JTWPA. (b),(c) Schematic and false-colored images of the QPA. The port at right (cyan) flux couples a pump tone to the JPA, producing on-chip amplification.

inequality to be nearly saturated. Here, however, on-chip amplification drives a second, parasitic measurement process in which $\hat{\sigma}_z$ information is encoded in other statistical moments of the output field. This dephasing mechanism is predicted to be independent of the mean field in the resonator, making it distinct from effects in resonantly current-pumped systems [27–32]. A rough heuristic model describes the parasitic measurement in two steps: The phase-sensitive on-chip gain squeezes the microwave vacuum noise, and the resultant output squeezed state is rotated in phase by the dispersive interaction, encoding $\hat{\sigma}_z$ information in the covariance of the output-field quadratures. These moments are largely not detected downstream, in part due to the fragility of the moments with respect to losses and in part because the phase-sensitive following JPA typically deamplifies this information. As the parasitic measurement increases Γ_ϕ without increasing the room-temperature SNR, it lowers η_{meas} .

Starting from Eq. (1), one can derive an expression for the parasitic dephasing rate (Appendix B and Ref. [26]):

$$\Gamma_{\phi, \text{parasitic}} = \frac{1}{2} \text{Re} \left[\sqrt{D(-\lambda)} + \sqrt{D(\lambda)} \right] - \frac{\kappa}{2} + 1/T_2^*. \quad (2)$$

Here, λ is related to the on-chip gain by

$$\lambda = \frac{\kappa \sqrt{G_{\text{QPA}} - 1}}{2 \sqrt{G_{\text{QPA}} + 1}}, \quad (3)$$

we define $D(\lambda) = (\kappa/2 + \lambda + i\chi)^2 - 2i\chi\lambda$, and T_2^* is an empirical parameter describing dephasing absent any applied drives. Several metrics are available to parametrize the gain dynamics; G_{QPA} indicates the (phase-preserving) power gain experienced by a tone slightly detuned from ω_{QPA} , which we measure directly using a vector network analyzer.

We characterize $\Gamma_{\phi, \text{parasitic}}$ via Ramsey oscillations of the qubit simultaneous with on-chip gain for several values of G_{QPA} . Absent any gain [Fig. 2(a), $G_{\text{QPA}} = 0$ dB], we observe $1/T_2^* = 0.23(7) \mu\text{s}^{-1}$. Applying pump power produces a squeezed vacuum inside the QPA, causing Γ_ϕ to increase significantly [Figs. 2(b) and 2(c)]. The inset ellipses in Fig. 2 indicate the quadrature variances and covariance (kurtosis is not shown) of the QPA output field predicted using equations from Ref. [26] and experimental parameters, colored red or blue depending on the qubit state. Increasing G_{QPA} decreases the overlap of the ellipses, speeding up the parasitic measurement. We find good agreement with the predictions of our zero-free parameter model over a range of G_{QPA} values as plotted in Fig. 2(d), supporting the validity of the model and indicating the absence of any comparable additional dephasing mechanism for these operating conditions.

A second set of Ramsey experiments illuminates how varying the on-chip gain modifies backaction during

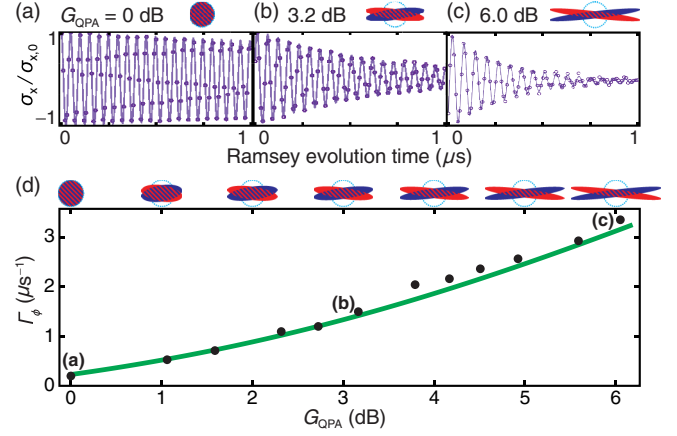


FIG. 2. (a)–(c) Ramsey experiments demonstrating the parasitic effect of on-chip gain G_{QPA} on qubit dephasing. No measurement tone is applied during the Ramsey free evolution. Increasing G_{QPA} increases the QPA output-field squeezing, thus decreasing the phase-space overlap of the output fields conditioned on the ground or excited qubit states as approximately represented by the red and blue ellipses. The decreased overlap implies faster parasitic dephasing. (d) The observed dependence of Γ_ϕ on G_{QPA} (black dots) is in good agreement with Eq. (2) (green curve); the thickness of the curve is the standard deviation of the background dephasing rate $1/T_2^*$.

an applied weak measurement. Our theory analysis (Appendix B and Ref. [26]) predicts the total dephasing to vary according to

$$\Gamma_\phi = \frac{2\chi^2 \kappa^2 P_{\text{in}}}{\hbar \omega_{\text{QPA}}} \left(\frac{\cos^2 \Phi}{|D(-\lambda)|^2} + \frac{\sin^2 \Phi}{|D(\lambda)|^2} \right) + \Gamma_{\phi, \text{parasitic}}, \quad (4)$$

where P_{in} is the power of the measurement tone incident to the QPA and $\Gamma_{\phi, \text{parasitic}}$ is, notably, still given by Eq. (2). Absent any on-chip gain ($\lambda = 0$), Eq. (4) can be approximated by the more standard expression $\Gamma_\phi = 8\chi^2 \bar{n} / \kappa + O(\chi/\kappa)^4$, describing dephasing induced as $\hat{\sigma}_z$ information is encoded in the phase of the QPA output field [Fig. 3(a), theory]. Experimentally, with $G_{\text{QPA}} = 0$ dB, we observe dephasing at rate $\Gamma_\phi = 0.49 \mu\text{s}^{-1}$ [Fig. 3(d)], from which we infer $P_{\text{in}} = -142$ dBm for this choice of drive. Keeping P_{in} fixed, we apply a flux pump such that $G_{\text{QPA}} = 3$ dB. Figures 3(b) and 3(c) show the expected output fields when the on-chip gain is aligned with ($\Phi = 0$) or orthogonal to ($\Phi = \pi/2$) the signal quadrature. The signal size ($\langle Q_e \rangle - \langle Q_g \rangle$) is nearly constant in all three cases: Since the input measurement drive lies along I while the output signal lies along Q , the net effects of amplification and deamplification approximately cancel. In contrast, the noise fluctuations do get amplified (squeezed), such that the SNR at the QPA output depends on Φ . Since amplifying the signal quadrature squeezes the photon number fluctuations in the conjugate quadrature which cause dephasing, we expect the amplifier mode ($\Phi = 0$) to minimize Γ_ϕ and the squeezer mode

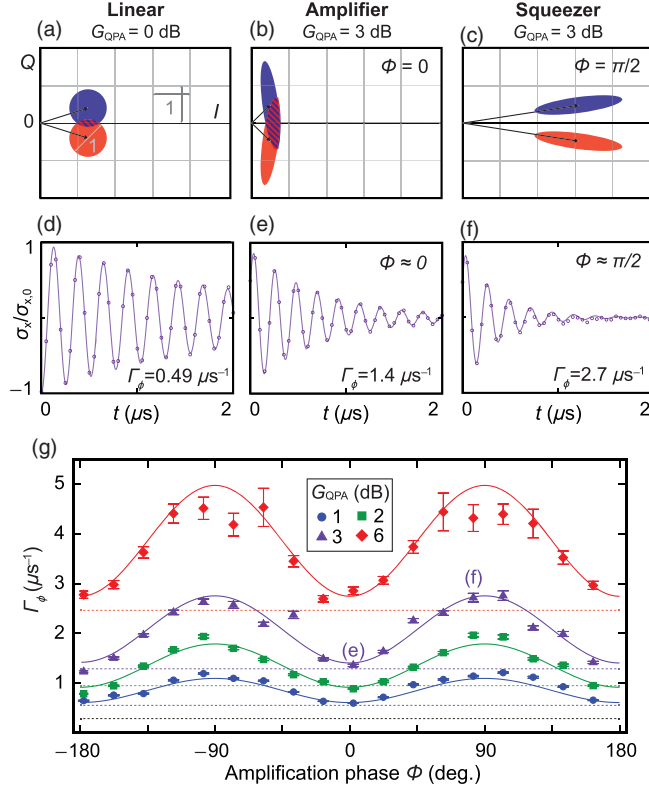


FIG. 3. (a)–(c) Approximate QPA output fields, calculated as in Fig. 2. (a) With no flux pump applied, a measurement tone reflected from the QPA acquires a $\hat{\sigma}_z$ -dependent phase rotation. (b) Applying a flux pump with phase $\Phi = 0$ amplifies the noise in the signal quadrature Q , reducing the output SNR but increasing robustness to off-chip losses. (c) The orthogonal choice $\Phi = \pi/2$ produces the opposite effects. The mean signal size is amplified slightly for either choice of Φ . (d)–(f) Ramsey experiments corresponding to the drive conditions used to calculate (a)–(c), exhibiting dephasing induced by a measurement tone applied during the Ramsey free evolution with (d) no on-chip gain, (e) amplifier-mode gain ($\Phi = 0$), or (f) squeezer-mode gain ($\Phi = \pi/2$). (g) Points indicate inferred Γ_ϕ values for a fixed measurement power (−142 dBm) over a range of pump settings. Colored dashed lines indicate $\Gamma_{\phi,\text{parasitic}}(G_{\text{QPA}})$; the black dashed line indicates $1/T_2^*$. Solid curves are a single fit to Eq. (4), where the only free parameter is a global phase. Dephasing is slowest (fastest) in the amplifier (squeezer) mode, where the SNR at the QPA output is lowest (greatest). We attribute the discrepancy at high gain and $\Phi \approx \pm\pi/2$ to higher-order nonlinearities driven by the large photon number at this condition.

($\Phi = \pi/2$) to maximize it, in agreement with the comparison in Figs. 3(e) and 3(f). Results of additional Ramsey measurements shown in Fig. 3(g) reveal the full dependence of Γ_ϕ on Φ and G_{QPA} and verify the predictions of our theory model [Eq. (4)]. We note that the squeezer mode is also of interest as a means of improving the SNR by reducing the quantum fluctuations of the output measurement field [26,33,34]; similar *in situ* squeezing generation has been demonstrated in a recent optical experiment [35].

Although the squeezer mode maximizes the SNR at the device output, the noise can never be reduced below what is added downstream. We henceforth focus exclusively on the amplifier mode ($\Phi = 0$). The primary benefit of the amplifier mode is that the noise floor of the QPA output signal quadrature is increased with minimal information loss, making the SNR insensitive to noise added downstream and enabling greater overall efficiency (for details, see Appendix B). A secondary effect is the deamplification of the mean field without deamplification of the signal; an interesting question is whether this effect, perhaps combined with an injected orthogonally squeezed vacuum, might enable a greater dispersive signal size for a fixed mean intracavity photon number.

III. MEASUREMENT EFFICIENCY

The total measurement efficiency is the product of on-chip efficiency and the efficiency of the rest of the measurement chain: $\eta_{\text{meas}} = \eta_{\text{QPA}}\eta_{\text{rest}}$. Increasing on-chip gain G_{QPA} increases η_{rest} , as the amplified signal quadrature becomes robust to losses, but decreases η_{QPA} due to the parasitic measurement discussed in Sec. II, such that there is an optimal G_{QPA} value maximizing η_{meas} for a given measurement drive. We can write the efficiency as the ratio of empirical quantities: $\eta_{\text{meas}} = \Gamma_{\text{meas}}/2\Gamma_\phi$. Here, $\Gamma_{\text{meas}} = [d/(dt)]\text{SNR}^2/4$ is the rate at which the square of the room-temperature voltage SNR increases with the integration time or, equivalently, the rate at which $\hat{\sigma}_z$ information is acquired by our digitizer.

In order to determine steady-state η_{meas} as a function of G_{QPA} and measurement drive $|\alpha_{\text{in}}| = \sqrt{P_{\text{in}}/\hbar\omega_{\text{QPA}}}$, we extract both Γ_{meas} and Γ_ϕ using the pulse sequence shown in Fig. 4(a). The flux pump is switched on in advance such that the mean intra-QPA field is deamplified along I at all times, reducing the intra-QPA circulating power produced by a strong measurement drive and thus helping to minimize undesired nonlinear processes in the QPA. Next, a continuous measurement tone is turned on and sufficient time allowed to pass to ensure the cavity has stabilized before a $\pi/2$ pulse is applied to initiate Ramsey evolution. After the second $\pi/2$, $|\alpha_{\text{in}}|$ is increased to perform a projective readout. The ensemble-averaged readout results for variable Ramsey evolution time are used to determine the dephasing rate Γ_ϕ , as in the right inset in Fig. 4(a). Integrating the steady-state weak-measurement record from the longest Ramsey evolution for a variable amount of time $t_{\text{int}} \leq 280$ ns and fitting Gaussians to the resultant histograms, we determine $\text{SNR}(t_{\text{int}})$ and thus Γ_{meas} . A modified Gaussian model adapted from Sec. III A in Ref. [36] is used to account for T_1 decay with T_1 fixed at the independently measured value above. Note that this treatment implicitly defines η_{meas} to be independent of relaxation events, such that a greater T_1 results in a higher readout fidelity but the same η_{meas} .

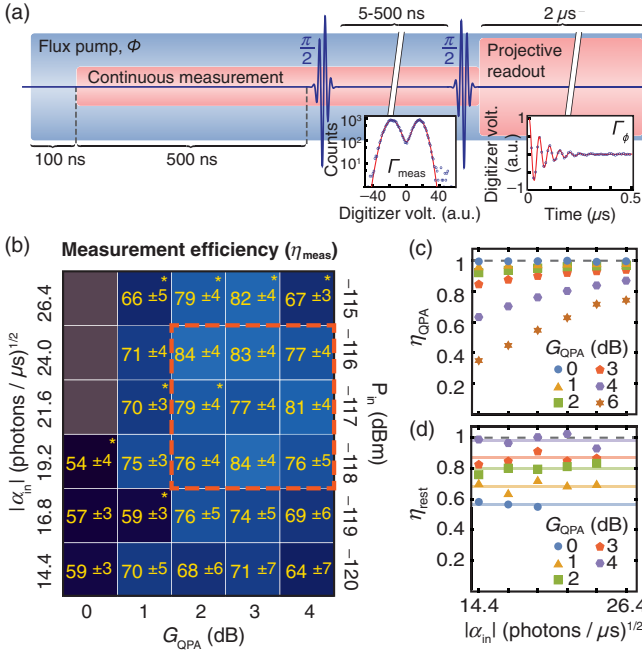


FIG. 4. (a) Ramsey sequence used to determine η_{meas} . Continuous measurement of the qubit causes dephasing at rate Γ_{ϕ} (right inset). Sampling the output measurement field during the Ramsey evolution yields histograms (left inset) from which we determine $\text{SNR}(t)$ and thus Γ_{meas} . (b) Inferred η_{meas} values as a function of G_{QPA} and continuous measurement amplitude $|\alpha_{\text{in}}|$. Settings marked with an asterisk produced a spurious third histogram peak containing $>1\%$ of the total events, which we attribute to large intra-QPA fields inducing transitions to the third transmon level. The dashed orange box surrounds the optimal operating region averaging $\eta_{\text{meas}} = 80\%$. (c) The on-chip efficiency η_{QPA} , inferred by comparing Γ_{ϕ} and $\Gamma_{\phi,\text{parasitic}}$, decreases with G_{QPA} and increases with $|\alpha_{\text{in}}|$. (d) The off-chip efficiency, inferred by dividing η (b) by η_{QPA} (c), increases with G_{QPA} and remains roughly constant for the shown $|\alpha_{\text{in}}|$ values. Horizontal lines mark mean values to guide the eye.

Sweeping the measurement strength and G_{QPA} , we find an ideal operating regime, indicated by the orange dashed box in Fig. 4(b), with an average $\eta_{\text{meas}} = 80\%$. To the left of the box, G_{QPA} is too low to mitigate the effect of loss in circulators and other off-chip components. The bottom edge of the box is defined by the decrease in η_{meas} associated with $\Gamma_{\phi,\text{parasitic}}$ becoming a larger fraction of Γ_{ϕ} as $|\alpha_{\text{in}}|$ is decreased. The other two sides of the box are marked by the onset of nonideal behavior evidenced by a third peak appearing in the measurement histograms. This spurious peak is not fully understood but seems to involve population of the third transmon level driven by large intra-QPA photon numbers occurring at too low or too high G_{QPA} (corresponding to a large mean field or a large field variance, respectively) or at too high $|\alpha_{\text{in}}|$.

With the assumption that $\Gamma_{\phi,\text{parasitic}}$ remains independent of $|\alpha_{\text{in}}|$ at this operating point, we can express the on-chip efficiency η_{QPA} in terms of empirical dephasing rates as

$\eta_{\text{QPA}} = 1 - \Gamma_{\phi,\text{parasitic}}/\Gamma_{\phi}$, from which we calculate the values shown in Fig. 4(c). In the absence of on-chip gain, η_{QPA} approaches unity as $\Gamma_{\phi,\text{parasitic}} = 1/T_2^* \ll \Gamma_{\phi}$. As gain is increased, $\Gamma_{\phi,\text{parasitic}}$ increases, resulting in lower η_{QPA} ; as the measurement strength is increased, the parasitic dephasing becomes less significant, increasing η_{QPA} . Calculating further, we can divide these values by the η_{meas} values in Fig. 4(b) to estimate η_{rest} , shown in Fig. 4(d). This plot is restricted to lower-power operating conditions in which the device is better behaved; over this domain, we infer that information loss downstream of the QPA decreases with G_{QPA} and is approximately independent of $|\alpha_{\text{in}}|$, supporting our previous assumption that $\Gamma_{\phi,\text{parasitic}}$ is likewise independent of $|\alpha_{\text{in}}|$. It is encouraging that the calculated values of η_{rest} approach 1 at $G_{\text{QPA}} = 4$ dB, though the current device does not permit increasing $|\alpha_{\text{in}}|$ sufficiently to maximally benefit from this much gain. We expect that this dynamic range ceiling, and thus η_{meas} , may be raised by reducing χ/κ and/or increasing the number of JPA SQUIDs [37,38], suppressing deleterious Kerr effects not included in our model.

IV. CONCLUSION

We have characterized the measurement backaction on a qubit dispersively coupled to a parametric amplifier flux pumped for gain, demonstrated how on-chip gain can mitigate off-chip sources of information loss, and observed steady-state efficiency η_{meas} up to 80%. Going forward, incremental improvements in η_{meas} may be achieved by further weakening device nonlinearities as discussed above to permit a larger measurement drive $|\alpha_{\text{in}}|$ and thus greater η_{QPA} . A more dramatic improvement might be realized by probing the device stroboscopically [4]. In a linear readout resonator, stroboscopic measurement has been shown to eliminate the undesired squeezing rotations caused by dispersive coupling [39]; realizing the analogous effect in the QPA would close the parasitic dephasing channel such that increasing G_{QPA} would boost η_{rest} without degrading η_{QPA} , even for small $|\alpha_{\text{in}}|$. Other potential near-term experiments include the exploration of effects of on-chip gain on initial transients when switching on a measurement and an investigation of whether combining the amplifier mode with an injected orthogonally squeezed vacuum enables a greater dispersive readout SNR for a fixed intracavity photon number. Longer term, we envision the QPA to be an enabling technology for applications demanding signal-to-noise ratios approaching the quantum limit, such as measurement-based quantum feedback [40–42] or further studies of individual quantum trajectories, perhaps with extension to multiqubit experiments via a chip layout similar to Ref. [16] followed by a broadband off-chip amplifier.

ACKNOWLEDGMENTS

The authors thank R. Vijay, S. Hacoen-Gourgy, E. Flurin, and L. Martin for useful discussions and thank

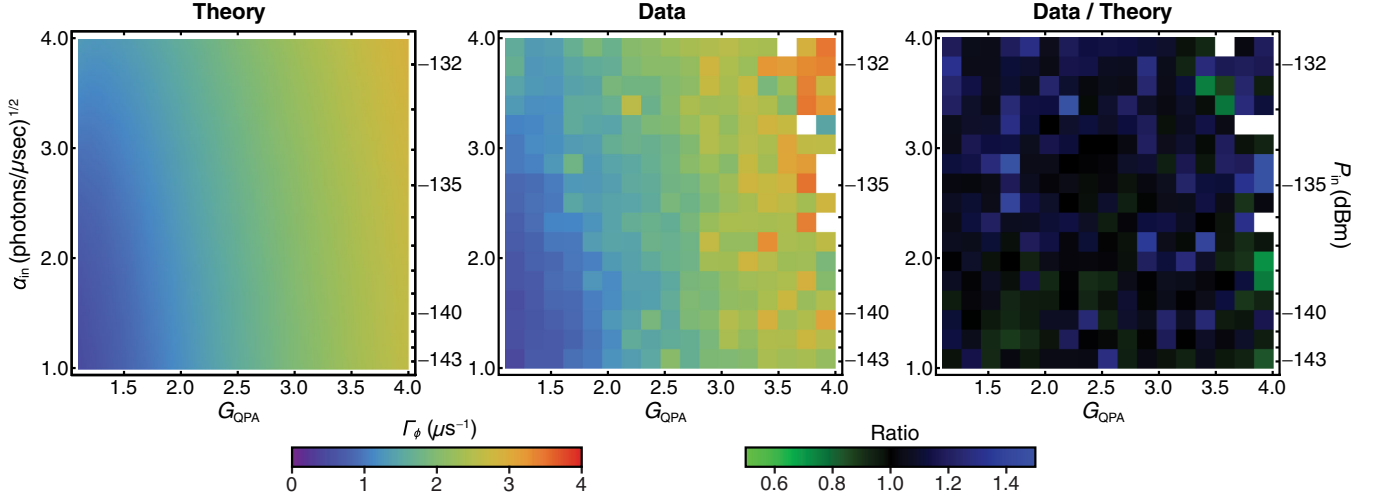


FIG. 6. Dephasing rate Γ_ϕ as a function of measurement strength $|\alpha_{\text{in}}|$ and on-chip gain G_{QPA} . The left panel shows the prediction of Eq. (4), while the central panel shows the Γ_ϕ values inferred from observation. The ratio of the data to the theory prediction is displayed in the right panel.

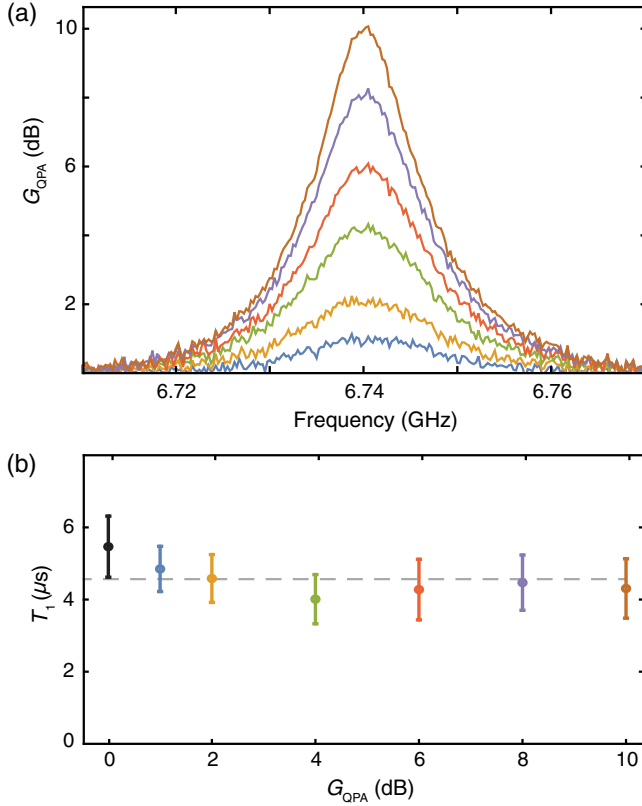


FIG. 7. (a) Gain profiles of the QPA for varying amounts of on-chip gain G_{QPA} as measured with a vector network analyzer. (b) Qubit T_1 measured at several values of G_{QPA} corresponding to the color-coded gain profiles in (a). Measurements are repeated for approximately 12 hr, during which time the order in which the gain settings are cycled through is repeatedly randomized. Error bars indicate the standard deviations of all results at each G_{QPA} setting.

the JTWPA became apparent at high JTWPA gain despite the intermediary low-pass filter, degrading JTWPA performance. These effects are suppressed by operating the JTWPA at a reduced gain (approximately 15 dB).

4. T_1 vs on-chip gain

We briefly investigate the effect of on-chip gain on the qubit lifetime T_1 . Results are shown in Fig. 7. The data suggest a small decrease in T_1 when gain is turned on, with no clear dependence as gain is further increased.

5. Amplifier-mode dephasing vs P_{in}

Extending the measurement-backaction data presented in Fig. 3, we fix the QPA pump phase to operate the QPA in the amplifier mode ($\Phi = 0$) and record Γ_ϕ for variable on-chip gain and measurement strength $|\alpha_{\text{in}}|$. The results are displayed alongside the theory prediction of Eq. (4) in Fig. 6. Good agreement is seen for low measurement strength and on-chip gain. At high drive strengths or high gains, excess dephasing is observed intermittently, i.e., for some experimental executions. At intermediate drive strength, near the center of the plot, this undesired behavior appears to be reduced as G_{QPA} increases from approximately 1 to approximately 2–3 dB.

APPENDIX B: THEORETICAL DERIVATIONS

1. Dephasing with on-chip gain

Our goal is to derive an analytic expression for the qubit dephasing rate in the long-time limit, without assuming that the dispersive coupling χ is weak. We start with the master equation

$$\dot{\hat{\rho}} = -i[\hat{H}, \hat{\rho}] + \kappa \mathcal{D}[\hat{a}]\hat{\rho} + \frac{1}{T_1} \mathcal{D}[\hat{\sigma}_-]\hat{\rho} + \frac{1}{2T_2} \mathcal{D}[\hat{\sigma}_z]\hat{\rho}, \quad (\text{B1})$$

where κ is the resonator decay rate, T_1 and T_2 are the relaxation and pure dephasing times of the qubit, respectively, $\hat{\sigma}_-$ is the qubit lowering operator, and $\mathcal{D}[\hat{O}]\hat{\rho} = \hat{O}\hat{\rho}\hat{O}^\dagger - \frac{1}{2}\{\hat{O}^\dagger\hat{O}, \hat{\rho}\}$ is the usual dissipator. In a frame where the qubit rotates at its bare frequency ω_q and the resonator at its static flux-biased frequency ω_{QPA} , the Hamiltonian is

$$\hat{H} = \frac{i\lambda}{2}(\hat{a}^{\dagger 2} - \hat{a}^2) + \chi \hat{a}^\dagger \hat{a} \hat{\sigma}_z + \sqrt{\kappa}(\alpha_{\text{in}} \hat{a}^\dagger + \alpha_{\text{in}}^* \hat{a}), \quad (\text{B2})$$

which contains the QPA dynamics of \hat{H}_{QPA} from Eq. (1) and the coherent measurement drive on the QPA resonator, characterized by the drive amplitude α_{in} .

The dephasing rate quantifies the decay of the qubit coherence in the long-time limit, described by the decay of the qubit off-diagonal matrix elements of the full density matrix. If we write the full density matrix as

$$\hat{\rho} = \sum_{\mu, \nu \in \{\uparrow, \downarrow\}} \hat{\rho}_{\mu\nu} \otimes |\mu\rangle\langle\nu|, \quad (\text{B3})$$

where $\hat{\rho}_{\mu\nu}$ is an operator on the resonator Hilbert space and $|\downarrow\rangle$ and $|\uparrow\rangle$ are the ground and excited states of the qubit, respectively, then the qubit dephasing rate is fully captured by the evolution of the part of the density matrix proportional to $|\uparrow\rangle\langle\downarrow|$ (or its Hermitian conjugate). Thus, we are interested in the evolution of the operator $\hat{\rho}_{\uparrow\downarrow}$. As is standard, we define the dephasing rate as

$$\Gamma_\phi = \lim_{t \rightarrow \infty} \frac{-\ln \{\text{Tr}[\hat{\rho}_{\uparrow\downarrow}(t)]\}}{t}, \quad (\text{B4})$$

which captures the exponential decay of the qubit coherence in the long-time limit.

From Eq. (B1), we calculate the evolution equation for the operator $\hat{\rho}_{\uparrow\downarrow}$:

$$\begin{aligned} \dot{\hat{\rho}}_{\uparrow\downarrow} = & \left[\frac{\lambda}{2}(\hat{a}^\dagger \hat{a}^\dagger - \hat{a} \hat{a}) - \sqrt{\kappa}(\alpha_{\text{in}} \hat{a}^\dagger - \alpha_{\text{in}}^* \hat{a}), \hat{\rho}_{\uparrow\downarrow} \right] \\ & - i\chi \{\hat{a}^\dagger \hat{a}, \hat{\rho}_{\uparrow\downarrow}\} + \kappa \mathcal{D}[\hat{a}]\hat{\rho}_{\uparrow\downarrow} - \left(\frac{1}{2T_1} + \frac{1}{T_2} \right) \hat{\rho}_{\uparrow\downarrow}. \end{aligned} \quad (\text{B5})$$

Note that this equation is not trace preserving, as it does not describe the evolution of a valid density matrix. Extending beyond the results of Ref. [26], we include the effect of qubit relaxation (T_1) in the evolution of $\hat{\rho}_{\uparrow\downarrow}$, and, while this effect means the evolution of the qubit is no longer quantum nondemolition (QND), the resulting equation for $\hat{\rho}_{\uparrow\downarrow}$ remains closed on itself and can be solved analytically.

The first step in solving Eq. (B5) is to remove the exponential decay caused by the qubit incoherent dynamics, and we do so by defining $\hat{\rho}'_{\uparrow\downarrow} = e^{t/T_2^*} \hat{\rho}_{\uparrow\downarrow}$, where $T_2^* = 2T_1 T_2 / (2T_1 + T_2)$ introduced in the main text describes the intrinsic dephasing of the qubit. The evolution equation for $\hat{\rho}'_{\uparrow\downarrow}$ describes the qubit dephasing due to interaction with the resonator and has the same form as Eq. (B5) but without the last term (proportional to $1/T_2^*$).

To solve the evolution equation for $\hat{\rho}'_{\uparrow\downarrow}$, it is more convenient to move to the Wigner representation and obtain a partial differential equation for $W_{\uparrow\downarrow}(x, p; t)$, the Wigner function representation of $\hat{\rho}'_{\uparrow\downarrow}$ [43]. As Eq. (B5) contains terms at most quadratic in \hat{a} and \hat{a}^\dagger , it is possible to solve this partial differential equation with a Gaussian ansatz.

The Gaussian ansatz reduces Eq. (B5) to a set of coupled ordinary differential equations for the means, variances, and overall norm of $\hat{\rho}'_{\uparrow\downarrow}$. After solving these in the steady state (see Ref. [26] for further details), with the coherent drive defined by

$$\alpha_{\text{in}} = \sqrt{\frac{P_{\text{in}}}{\hbar\omega_{\text{QPA}}}} [\cos(\Phi) + i \sin(\Phi)], \quad (\text{B6})$$

we can then use Eq. (B4) to define the dephasing rate, which gives the expression found in Eq. (4). (By defining $|\alpha_{\text{in}}|$ in terms of Φ here, we implicitly fix the phase of the pump, in contrast to the convention used in the main text).

2. Measurement rate with on-chip gain

We now briefly outline the theoretical calculations of the measurement rate, and for further details the interested reader should consult Chap. 3 in Ref. [26]. From standard input-output theory, the Heisenberg-Langevin equation for the resonator operator \hat{a} in a frame rotating at the bare resonator frequency ω_{QPA} is

$$\dot{\hat{a}} = \left(-i\chi \hat{\sigma}_z - \frac{\kappa}{2} \right) \hat{a} + \lambda \hat{a}^\dagger - \sqrt{\kappa} \hat{a}_{\text{in}}, \quad (\text{B7})$$

where \hat{a}_{in} is the input field to the resonator. In our case, for dispersive measurement of the qubit, this is ideally a coherent state, such that $\langle \hat{a}_{\text{in}} \rangle = \alpha_{\text{in}}$, with α_{in} defined in Eq. (B6). For the purposes of the intracavity dynamics and calculation of the measurement rate, we can treat the qubit operator $\hat{\sigma}_z$ as a classical real variable $\sigma = \pm 1$, corresponding to the ground or excited state of the qubit in the $\hat{\sigma}_z$ basis. Doing so allows us to solve Eq. (B7) exactly and from this solution extract the measurement rate.

We consider two modes of operation for the QPA: the ‘‘amplifier mode,’’ where the input field aligns with the direction of squeezing ($\Phi = 0$), and the ‘‘squeezer mode,’’ where the input field aligns with the direction of amplification ($\Phi = \pi/2$). In the amplifier mode, we use the QPA

to amplify the size of the signal created by the qubit, which comes at the cost of also amplifying the noise in the cavity output field. In the squeezer mode, we use the QPA to squeeze the noise in the quadrature containing qubit information, and, while the noise can be heavily squeezed, the signal produced by the qubit is squeezed only at most by a factor of 2. For a fixed input photon flux, the steady-state intracavity photon number is not the same for both modes of operation but is independent of the qubit state in both cases.

The output field is related to the input field by the standard input-output relation $\hat{a}_{\text{out}} = \hat{a}_{\text{in}} + \sqrt{\kappa}\hat{a}$, and from the output mode we define the measured signal operator by

$$\hat{Q}(t) = \frac{e^{-i\delta}\hat{a}_{\text{out}} + e^{i\delta}\hat{a}_{\text{out}}^\dagger}{\sqrt{2}}, \quad (\text{B8})$$

where the angle δ parametrizes the quadrature measured. We must choose the measured quadrature such that it is out of phase with the input coherent signal (as the qubit information is contained in the out-of-phase quadrature) such that $|\delta - \Phi| = \pi/2$.

As we are interested in the long-time limit of the QPA dynamics, rather than the SNR we calculate the measurement rate, defined by

$$\Gamma_{\text{meas}} \equiv \lim_{\tau \rightarrow \infty} \frac{\text{SNR}^2(\tau)}{2\tau} = \frac{1}{4} \frac{(\langle \hat{Q} \rangle_\uparrow - \langle \hat{Q} \rangle_\downarrow)^2}{(\bar{S}_{\text{QO},\uparrow}[0] + \bar{S}_{\text{QO},\downarrow}[0])}, \quad (\text{B9})$$

where $\langle \cdot \rangle_\nu$ indicates that the expectation value is taken with respect to the cavity in the steady state and the qubit in state $|\nu\rangle$ for $\nu \in \{\uparrow, \downarrow\}$, corresponding to $\sigma = \pm 1$, respectively. $\bar{S}_{\text{QO},\nu}[\omega]$ is the symmetrized noise power of the detected quadrature at frequency ω , defined in the standard way [26].

The measurement rate depends on what mode the QPA is operated in (i.e., the angle Φ), and for our two operation modes the measurement rates are

$$\Gamma_{\text{meas}}^{\text{amp}} = \frac{\frac{\chi^2 \kappa |\alpha|^2}{(\frac{\kappa}{2} - \lambda)^2 + \chi^2}}{\frac{1}{2} \frac{[(\frac{\kappa}{2} + \lambda)^2 - \chi^2]^2 + \chi^2 \kappa^2}{(\frac{\kappa}{2} - \lambda)^2 + \chi^2} + \bar{n}_{\text{add}}}, \quad (\text{B10})$$

$$\Gamma_{\text{meas}}^{\text{sqz}} = \frac{\frac{\chi^2 \kappa |\alpha|^2}{(\frac{\kappa}{2} + \lambda)^2 + \chi^2}}{\frac{1}{2} \frac{[(\frac{\kappa}{2} - \lambda)^2 - \chi^2]^2 + \chi^2 \kappa^2}{(\frac{\kappa}{2} - \lambda)^2 + \chi^2} + \bar{n}_{\text{add}}}, \quad (\text{B11})$$

respectively, where we add by hand a noise term \bar{n}_{add} to quantify noise added to the signal downstream of the QPA. For a fair comparison, we parametrize the rates in terms of a constant intracavity photon number $|\alpha|^2$, which we note requires different input photon flux for the two operation modes.

From Eqs. (B10) and (B11), we see that in both modes of operation the output contains amplified noise, even for small nonzero λ . While this noise is by design in the amplifier mode, in the squeezer mode it is naively unexpected and is a result of interaction with the qubit. The dispersive interaction results in a qubit-dependent phase shift on the field exiting the resonator such that it no longer perfectly interferes with the promptly reflected field. The effect of this shift is a mixing of the squeezed and amplified noise such that all quadratures contain noise contributions from both.

However, for very small χ/κ , squeezer mode operation does not suffer from this unwanted mixed-in amplified noise, as can be seen when we write the measurement rates to leading order in χ/κ :

$$\Gamma_{\text{meas}}^{\text{amp}} \approx \frac{2\chi^2 |\alpha|^2 (1 + \sqrt{G_0})^2}{\kappa(G_0 + 2\bar{n}_{\text{add}})}, \quad (\text{B12})$$

$$\Gamma_{\text{meas}}^{\text{sqz}} \approx \frac{2\chi^2 |\alpha|^2 (1 + 1/\sqrt{G_0})^2}{\kappa(1/G_0 + 2\bar{n}_{\text{add}})}, \quad (\text{B13})$$

where we define $\sqrt{G_0} = (\kappa/2 + \lambda)/(\kappa/2 - \lambda)$, with $G_0 = 1$ for zero gain. Both measurement rates should be contrasted with the zero gain measurement rate

$$\Gamma_{\text{meas}}^0 = \frac{2\chi^2 \kappa |\alpha|^2}{(\frac{\kappa^2}{4} + \chi^2)[1 + 2\bar{n}_{\text{add}}]} \xrightarrow{\chi/\kappa \ll 1} \frac{8\chi^2 |\alpha|^2}{\kappa(1 + 2\bar{n}_{\text{add}})}, \quad (\text{B14})$$

found for a standard linear-resonator setup, or when the QPA is operated with zero gain.

In the ideal limit, where $\bar{n}_{\text{add}} = 0$, the amplifier mode offers little to no advantage over zero gain, as both the signal and noise are amplified by the same factor at a large gain, which can be seen by comparing Eq. (B12) for $\bar{n}_{\text{add}} = 0$ to Eq. (B14). However, in this case, the squeezer mode can be advantageous, as in the large gain limit the noise is drastically reduced, while the signal is relatively unaffected. In particular, for $\chi/\kappa \ll 1$, comparing Eq. (B13) for $\bar{n}_{\text{add}} = 0$ to Eq. (B14), we see that the measurement rate is enhanced by a large factor proportional to G_0 . Accounting for effects beyond first order in χ/κ by using the full expression of Eq. (B11), we find that the squeezer mode measurement rate is enhanced by the factor $\Gamma_{\text{meas}}^{\text{sqz}}/\Gamma_{\text{meas}}^0 = \kappa/\chi$ at the optimal value of λ .

Conversely, in the nonideal situation where \bar{n}_{add} is large, the squeezer mode offers no advantage, as the noise can never be reduced below the noise floor set by \bar{n}_{add} , as clearly indicated by Eq. (B13). In this situation, the amplifier mode is beneficial, as, by amplifying both the signal and noise leaving the QPA, the output becomes insensitive to noise added downstream [concretely, $G_0 \gg \bar{n}_{\text{add}}$ in the denominator in Eq. (B12)]. As shown in the main text, this is the mode of operation we find gives the greatest efficiency for our current setup.

- [1] R. Vijay, C. Macklin, D. H. Slichter, S. J. Weber, K. W. Murch, R. Naik, A. N. Korotkov, and I. Siddiqi, *Stabilizing Rabi Oscillations in a Superconducting Qubit Using Quantum Feedback*, *Nature (London)* **490**, 77 (2012).
- [2] K. W. Murch, S. J. Weber, C. Macklin, and I. Siddiqi, *Observing Single Quantum Trajectories of a Superconducting Quantum Bit*, *Nature (London)* **502**, 211 (2013).
- [3] S. J. Weber, A. Chantasri, J. Dressel, A. N. Jordan, K. W. Murch, and I. Siddiqi, *Mapping the Optimal Route between Two Quantum States*, *Nature (London)* **511**, 570 (2014).
- [4] S. Hacohen-Gourgy, L. S. Martin, E. Flurin, V. V. Ramasesh, K. B. Whaley, and I. Siddiqi, *Quantum Dynamics of Simultaneously Measured Non-Commuting Observables*, *Nature (London)* **538**, 491 (2016).
- [5] P. Campagne-Ibarcq, P. Six, L. Bretheau, A. Sarlette, M. Mirrahimi, P. Rouchon, and B. Huard, *Observing Quantum State Diffusion by Heterodyne Detection of Fluorescence*, *Phys. Rev. X* **6**, 011002 (2016).
- [6] Q. Ficheux, S. Jezouin, Z. Leghtas, and B. Huard, *Dynamics of a Qubit while Simultaneously Monitoring Its Relaxation and Dephasing*, *Nat. Commun.* **9**, 1926 (2018).
- [7] T. Walter, P. Kurpiers, S. Gasparinetti, P. Magnard, A. Potočník, Y. Salathé, M. Pechal, M. Mondal, M. Oppliger, C. Eichler, and A. Wallraff, *Rapid High-Fidelity Single-Shot Dispersive Readout of Superconducting Qubits*, *Phys. Rev. Applied* **7**, 054020 (2017).
- [8] B. J. Chapman, E. I. Rosenthal, J. Kerckhoff, B. A. Moores, L. R. Vale, J. A. B. Mates, G. C. Hilton, K. Lalumière, A. Blais, and K. W. Lehnert, *Widely Tunable On-Chip Microwave Circulator for Superconducting Quantum Circuits*, *Phys. Rev. X* **7**, 041043 (2017).
- [9] F. Lecocq, L. Ranzani, G. A. Peterson, K. Cicak, R. W. Simmonds, J. D. Teufel, and J. Aumentado, *Nonreciprocal Microwave Signal Processing with a Field-Programmable Josephson Amplifier*, *Phys. Rev. Applied* **7**, 024028 (2017).
- [10] G. A. Peterson, F. Lecocq, K. Cicak, R. W. Simmonds, J. Aumentado, and J. D. Teufel, *Demonstration of Efficient Nonreciprocity in a Microwave Optomechanical Circuit*, *Phys. Rev. X* **7**, 031001 (2017).
- [11] K. M. Sliwa, M. Hatridge, A. Narla, S. Shankar, L. Frunzio, R. J. Schoelkopf, and M. H. Devoret, *Reconfigurable Josephson Circulator/Directional Amplifier*, *Phys. Rev. X* **5**, 041020 (2015).
- [12] J. Kerckhoff, K. Lalumière, B. J. Chapman, A. Blais, and K. W. Lehnert, *On-Chip Superconducting Microwave Circulator from Synthetic Rotation*, *Phys. Rev. Applied* **4**, 034002 (2015).
- [13] L. Ranzani, S. Kotler, A. J. Sirois, M. P. DeFeo, M. Castellanos-Beltran, K. Cicak, L. R. Vale, and J. Aumentado, *Wideband Isolation by Frequency Conversion in a Josephson-Junction Transmission Line*, *Phys. Rev. Applied* **8**, 054035 (2017).
- [14] A. Metelmann and A. A. Clerk, *Nonreciprocal Photon Transmission and Amplification via Reservoir Engineering*, *Phys. Rev. X* **5**, 021025 (2015).
- [15] I. Siddiqi, R. Vijay, F. Pierre, C. M. Wilson, M. Metcalfe, C. Rigetti, L. Frunzio, and M. H. Devoret, *RF-Driven Josephson Bifurcation Amplifier for Quantum Measurement*, *Phys. Rev. Lett.* **93**, 207002 (2004).
- [16] V. Schmitt, X. Zhou, K. Juliusson, B. Royer, A. Blais, P. Bertet, D. Vion, and D. Esteve, *Multiplexed Readout of Transmon Qubits with Josephson Bifurcation Amplifiers*, *Phys. Rev. A* **90**, 062333 (2014).
- [17] P. Krantz, A. Bengtsson, M. Simoen, S. Gustavsson, V. Shumeiko, W. D. Oliver, C. M. Wilson, P. Delsing, and J. Bylander, *Single-Shot Read-Out of a Superconducting Qubit Using a Josephson Parametric Oscillator*, *Nat. Commun.* **7**, 11417 (2016).
- [18] C. Ahn, A. C. Doherty, and A. J. Landahl, *Continuous Quantum Error Correction via Quantum Feedback Control*, *Phys. Rev. A* **65**, 042301 (2002).
- [19] M. Naghiloo, A. N. Jordan, and K. W. Murch, *Achieving Optimal Quantum Acceleration of Frequency Estimation Using Adaptive Coherent Control*, *Phys. Rev. Lett.* **119**, 180801 (2017).
- [20] C. Leroux, L. C. G. Govia, and A. A. Clerk, *Enhancing Cavity Quantum Electrodynamics via Antisqueezing: Synthetic Ultrastrong Coupling*, *Phys. Rev. Lett.* **120**, 093602 (2018).
- [21] J. Koch, T. M. Yu, J. Gambetta, A. A. Houck, D. I. Schuster, J. Majer, A. Blais, M. H. Devoret, S. M. Girvin, and R. J. Schoelkopf, *Charge-Insensitive Qubit Design Derived from the Cooper Pair Box*, *Phys. Rev. A* **76**, 042319 (2007).
- [22] C. Macklin, K. O'Brien, D. Hover, M. E. Schwartz, V. Bolkhovskoy, X. Zhang, W. D. Oliver, and I. Siddiqi, *A Near Quantum-Limited Josephson Traveling-Wave Parametric Amplifier*, *Science* **350**, 307 (2015).
- [23] D. M. Toyli, A. W. Eddins, S. Boutin, S. Puri, D. Hover, V. Bolkhovskoy, W. D. Oliver, A. Blais, and I. Siddiqi, *Resonance Fluorescence from an Artificial Atom in Squeezed Vacuum*, *Phys. Rev. X* **6**, 031004 (2016).
- [24] X. Zhou, V. Schmitt, P. Bertet, D. Vion, W. Wustmann, V. Shumeiko, and D. Esteve, *High-Gain Weakly Nonlinear Flux-Modulated Josephson Parametric Amplifier Using a SQUID Array*, *Phys. Rev. B* **89**, 214517 (2014).
- [25] M. D. Reed, B. R. Johnson, A. A. Houck, L. DiCarlo, J. M. Chow, D. I. Schuster, L. Frunzio, and R. J. Schoelkopf, *Fast Reset and Suppressing Spontaneous Emission of a Superconducting Qubit*, *Appl. Phys. Lett.* **96**, 203110 (2010).
- [26] B. Levitan, *Dispersive Qubit Measurement Using an On-Chip Parametric Amplifier*, Master's thesis, McGill University, 2015.
- [27] F. R. Ong, M. Boissonneault, F. Mallet, A. Palacios-Laloy, A. Dewes, A. C. Doherty, A. Blais, P. Bertet, D. Vion, and D. Esteve, *Circuit QED with a Nonlinear Resonator: ac-Stark Shift and Dephasing*, *Phys. Rev. Lett.* **106**, 167002 (2011).
- [28] M. Boissonneault, A. C. Doherty, F. R. Ong, P. Bertet, D. Vion, D. Esteve, and A. Blais, *Back-Action of a Driven Nonlinear Resonator on a Superconducting Qubit*, *Phys. Rev. A* **85**, 022305 (2012).
- [29] F. R. Ong, M. Boissonneault, F. Mallet, A. C. Doherty, A. Blais, D. Vion, D. Esteve, and P. Bertet, *Quantum Heating of a Nonlinear Resonator Probed by a Superconducting Qubit*, *Phys. Rev. Lett.* **110**, 047001 (2013).
- [30] M. Boissonneault, A. C. Doherty, F. R. Ong, P. Bertet, D. Vion, D. Esteve, and A. Blais, *Superconducting Qubit as a Probe of Squeezing in a Nonlinear Resonator*, *Phys. Rev. A* **89**, 022324 (2014).

- [31] M. Hatridge, R. Vijay, D. H. Slichter, J. Clarke, and I. Siddiqi, *Dispersive Magnetometry with a Quantum Limited SQUID Parametric Amplifier*, *Phys. Rev. B* **83**, 134501 (2011).
- [32] E. M. Levenson-Falk, R. Vijay, N. Antler, and I. Siddiqi, *A Dispersive Nanosquid Magnetometer for Ultra-Low Noise, High Bandwidth Flux Detection*, *Supercond. Sci. Technol.* **26**, 055015 (2013).
- [33] V. Peano, H. G. L. Schwefel, C. Marquardt, and F. Marquardt, *Intracavity Squeezing Can Enhance Quantum-Limited Optomechanical Position Detection through Deamplification*, *Phys. Rev. Lett.* **115**, 243603 (2015).
- [34] L. C. G. Govia and A. A. Clerk, *Enhanced Qubit Readout Using Locally Generated Squeezing and Inbuilt Purcell-Decay Suppression*, *New J. Phys.* **19**, 023044 (2017).
- [35] M. Korobko, L. Kleybolte, S. Ast, H. Miao, Y. Chen, and R. Schnabel, *Beating the Standard Sensitivity-Bandwidth Limit of Cavity-Enhanced Interferometers with Internal Squeezed-Light Generation*, *Phys. Rev. Lett.* **118**, 143601 (2017).
- [36] J. Gambetta, W. A. Braff, A. Wallraff, S. M. Girvin, and R. J. Schoelkopf, *Protocols for Optimal Readout of Qubits Using a Continuous Quantum Nondemolition Measurement*, *Phys. Rev. A* **76**, 012325 (2007).
- [37] C. Eichler and A. Wallraff, *Controlling the Dynamic Range of a Josephson Parametric Amplifier*, *EPJ Quantum Technol.* **1**, 2 (2014).
- [38] S. Boutin, D. M. Toyli, A. V. Venkatramani, A. W. Eddins, I. Siddiqi, and A. Blais, *Effect of Higher-Order Nonlinearities on Amplification and Squeezing in Josephson Parametric Amplifiers*, *Phys. Rev. Applied* **8**, 054030 (2017).
- [39] A. Eddins, S. Schreppler, D. M. Toyli, L. S. Martin, S. Hacoen-Gourgy, L. C. G. Govia, H. Ribeiro, A. A. Clerk, and I. Siddiqi, *Stroboscopic Qubit Measurement with Squeezed Illumination*, arXiv:1708.01674.
- [40] H. Li, A. Shabani, M. Sarovar, and K. B. Whaley, *Optimality of Qubit Purification Protocols in the Presence of Imperfections*, *Phys. Rev. A* **87**, 032334 (2013).
- [41] L. Martin, F. Motzoi, H. Li, M. Sarovar, and K. B. Whaley, *Deterministic Generation of Remote Entanglement with Active Quantum Feedback*, *Phys. Rev. A* **92**, 062321 (2015).
- [42] L. Martin, M. Sayrafi, and K. B. Whaley, *What Is the Optimal Way to Prepare a Bell State Using Measurement and Feedback?*, *Quantum Sci. Technol.* **2**, 044006 (2017).
- [43] D. W. Utami and A. A. Clerk, *Entanglement Dynamics in a Dispersively Coupled Qubit-Oscillator System*, *Phys. Rev. A* **78**, 042323 (2008).